Inorg. Chem. **2009**, *48*, 466−475

Lanthanide(III) Complexes of Pyridine-*N*-Oxide Analogues of DOTA in Solution and in the Solid State. A New Kind of Isomerism in Complexes of DOTA-like Ligands†

Miloslav Polášek,‡ Jan Kotek,‡ Petr Hermann,*,‡ Ivana Císařová,‡ Koen Binnemans,§ and Ivan Lukeš‡

Department of Inorganic Chemistry, Charles University, Hlavova 2030, 128 40 Prague 2, Czech Republic, and Department of Chemistry, Katholieke Universiteit Leuven, Celestijnenlaan 200F, B-3001 Leuven, Belgium

Received August 21, 2008

The replacement of one of the acetate pendant arms with a 2-methylpyridine-*N*-oxide group in the molecule of H_4dota significantly alters the coordination properties of the ligand in Ln^{III} complexes. The structural properties of the complexes are investigated both in solution and in the solid state. The variable-temperature ^{1}H NMR spectra of Nd^{III}, Eu^{III}, and Yb^{III} complexes show that the twisted-square-antiprismatic (TSA) isomer is strongly destabilized and suppressed in solution and the complexes exist mostly as the square-antiprismatic (SA) isomers (98% for Eu^{III} at −35 °C). The exchange between the TSA and SA isomers is fast at room temperature compared to that of the NMR time scale. The flexibility of the six-membered chelate ring formed by coordination of the 2-methylpyridine-*N*-oxide group to the central ion allows two orientations of this pendant arm relative to the acetate arms: *syn*-SA (pyridine in the direction of the acetates) and *anti*-SA (pyridine opposite to the acetates). The *syn*-SA form was found in the X-ray structure of the Nd^{III} complex; the *anti*-SA forms were found in the structures of Dy^{III}, Tm^{III}, and Yb^{III} complexes. The UV−vis and ^{1}H NMR spectra of the Eu^{III} complex suggest that both forms are in dynamic equilibrium in solution. A derivatization of the pyridine-*N*-oxide group with a carboxylic group in the 4 position has no significant effect on the properties of the Ln^{III} complexes.

Introduction

The monohydrated Gd^{III} complexes of poly(aminocarboxylates) have been intensively studied in the past few decades for their use as contrast agents (CAs) for magnetic resonance imaging (MRI). A typical example of the appropriate chelators developed for this purpose is the macrocyclic DOTA (Chart 1), which also represents a template for designing many other compounds. Thorough investigations of a large variety of related compounds[1] have revealed the basic relationships between the molecular structure of ligands/complexes and the function of CAs. This understanding brought new possibilities to improving the relatively low efficiency of the first-generation CAs by the rational design of the ligand molecule. One of the most difficult tasks encountered in the development of high-efficiency CAs is the optimization of the exchange rate of the water molecule coordinated to the Gd^{III} ion with the bulk molecules. To obtain an optimum, the values of this parameter can be varied between narrow margins only, and most of the CAs exhibit much slower exchange rates.[2] The factors affecting the water exchange are mainly the overall charge of the complex[3] and the steric strain at the water-binding site.[4] Because variation of the charge gives only limited options and intravenous application of highly charged chelates is problematic, the focus was turned to tuning of the steric strain. The water

† Dedicated to Dr. Joop A. Peters (Delft University of Technology, Delft, The Netherlands) on the occasion of his 65th birthday in appreciation of his contribution in the field of NMR investigation of lanthanide complexes.

* To whom correspondence should be addressed. E-mail: petrh@natur.cuni.cz. Tel: (+420)22195-1263. Fax: (+420)22195-1253.

‡ Charles University.

§ Katholieke Universiteit Leuven.

(1) Caravan, P.; Ellison, J. J.; McMurry, T. J.; Lauffer, R. B. *Chem. Rev.* **1999**, *99*, 2293–2352.

(2) Aime, S.; Botta, M.; Fasano, M.; Terreno, E. *Chem. Soc. Rev.* **1998**, *27*, 19–29.

(3) (a) André, J. P.; Maecke, H. R.; Tóth, É.; Merbach, A. E. *J. Biol. Inorg. Chem.* **1999**, *4*, 341–347. (b) Tóth, É.; Vauthey, S.; Pubanz, D.; Merbach, A. E. *Inorg. Chem.* **1996**, *35*, 3375–3379. (c) Zhang, S.; Jiang, X.; Sherry, A. D. *Helv. Chim. Acta* **2005**, *88*, 923–935.

(4) Parker, D.; Puschmann, H.; Batsanov, A. S.; Senanayake, K. *Inorg. Chem.* **2003**, *42*, 8646–8651.

10.1021/ic801597z CCC: $40.75
Published on Web 12/16/2008

Chart 1. Structures of the Ligands Discussed in This Work

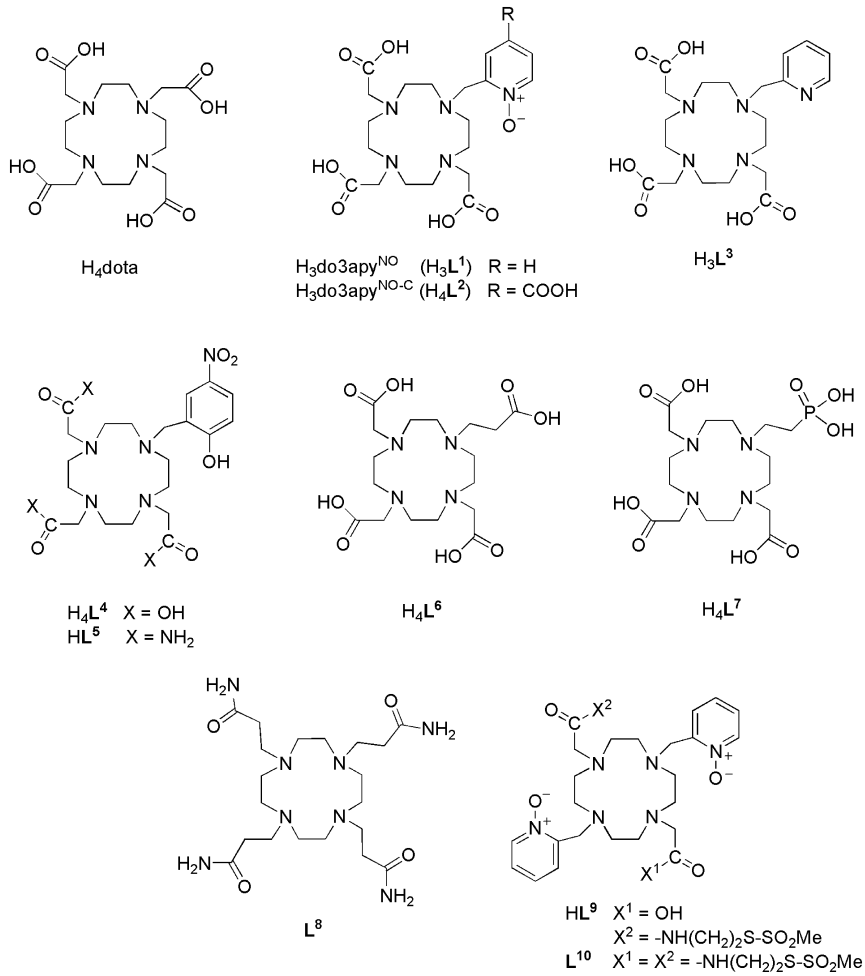

exchange in monohydrated Ln^{III} complexes of DOTA-like ligands is achieved via dissociative, D, or dissociative interchange, I_D, mechanisms.[5] Thus, a slightly increased steric strain at the water-binding site facilitates the dissociation of the water molecule and, hence, increases the exchange rate. The steric strain can be modulated either directly or indirectly, depending on the method of modification of the ligand. The direct approach utilizes sterically more demanding pendant arms[6] or produces the steric strain by increasing the number of atoms in the chelate rings formed by the pendant arms[7,8] or by the macrocycle.[9] The steric strain can also be controlled indirectly through isomerism of the complexes. It is known that the coordination of DOTA or related octadentate ligands to the Ln^{III} ions results in two stable arrangements, a square antiprism (SA) and a twisted square antiprism (TSA).[10] This isomerism is enabled by two possible configurations of the chelate rings of the macrocycle ($\lambda\lambda\lambda\lambda$ and $\delta\delta\delta\delta$) and two orientations of the pendant arms (Δ and Λ). The enantiomers $\Delta\lambda\lambda\lambda\lambda$ and $\Lambda\delta\delta\delta\delta$ adopt the SA structures, while the pair of $\Lambda\lambda\lambda\lambda\lambda$ and $\Delta\delta\delta\delta\delta$ forms the TSA arrangement (Figure 1). The water exchange rate in the TSA isomer was found to be approximately 50 times faster than that in the SA isomer[11] and, hence, ways to favor the formation of the TSA isomer have been pursued. Normally, the isomers exist in a dynamic equilibrium achieved by an inversion of the macrocycle and a rotation of the pendant arms. However, a proper modification of the ligand backbone can block these processes and, thus, lock

(5) Merbach, A. E.; Tóth, É. *The Chemistry of Contrast Agents in Medical Magnetic Resonance Imaging*; John Wiley & Sons: Chichester, U.K., 2001.

(6) (a) Rudovský, J.; Kotek, J.; Hermann, P.; Lukeš, I.; Mainero, V.; Aime, S. *Org. Biomol. Chem.* **2005**, *3*, 112–117. (b) Rudovský, J.; Cígler, P.; Kotek, J.; Hermann, P.; Vojtíšek, P.; Lukeš, I.; Peters, J. A.; Elst, L. V.; Muller, R. N. *Chem.—Eur. J.* **2005**, *11*, 2373–2384. (c) Rudovský, J.; Botta, M.; Hermann, P.; Koridze, A.; Aime, S. *Dalton Trans.* **2006**, 2323–2333. (d) Lebdušková, P.; Hermann, P.; Helm, L.; Tóth, É.; Kotek, J.; Binnemans, K.; Rudovský, J.; Lukeš, I.; Merbach, A. E. *Dalton Trans.* **2007**, 493–501.

(7) Congreve, A.; Parker, D.; Gianolio, E.; Botta, M. *Dalton Trans.* **2004**, 1441–1445.

(8) Jászberényi, Z.; Sour, A.; Tóth, É.; Benmelouka, M.; Merbach, A. E. *Dalton Trans.* **2005**, 2713–2719.

(9) (a) Ruloff, R.; Tóth, É.; Scopelliti, R.; Tripier, R.; Handel, H.; Merbach, A. E. *Chem. Commun.* **2002**, 2630–2631. (b) Laus, S.; Ruloff, R.; Tóth, É.; Merbach, A. E. *Chem.—Eur. J.* **2003**, *9*, 3555–3566.

(10) (a) Aime, S.; Botta, M.; Ermondi, G. *Inorg. Chem.* **1992**, *31*, 4291–4299. (b) Aime, S.; Botta, M.; Fasano, M.; Marques, M. P. M.; Geraldes, C. F. G. C.; Pubanz, D.; Merbach, A. E. *Inorg. Chem.* **1997**, *36*, 2059–2068. (c) Hoeft, S.; Roth, K. *Chem. Ber.* **1993**, *126*, 869–873.

(11) (a) Aime, S.; Barge, A.; Botta, M.; De Sousa, A. S.; Parker, D. *Angew. Chem., Int. Ed.* **1998**, *37*, 2673–2675. (b) Dunand, F. A.; Aime, S.; Merbach, A. E. *J. Am. Chem. Soc.* **2000**, *122*, 1506–1512. (c) Zhang, S. R.; Kovacs, Z.; Burgess, S.; Aime, S.; Terreno, E.; Sherry, A. D. *Chem.—Eur. J.* **2001**, *7*, 288–296. (d) Dunand, F. A.; Dickins, R. S.; Parker, D.; Merbach, A. E. *Chem.—Eur. J.* **2001**, *7*, 5160–5167.

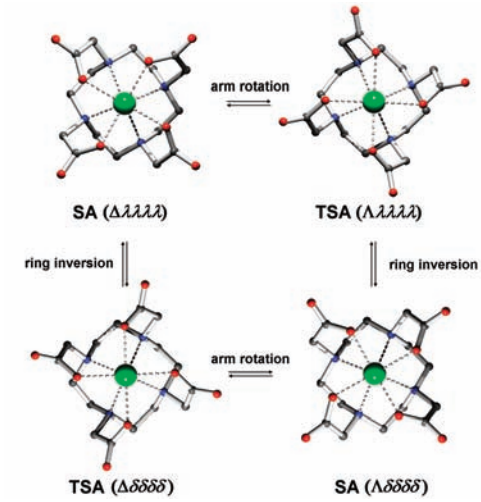

Figure 1. Isomerism of complexes with DOTA-like ligands.

the geometry in either the TSA or SA arrangement.[12] The directed formation of the TSA isomer leads to a successful acceleration of the water exchange, but the complicated stereospecific synthesis of suitable ligands is a substantial drawback of this approach. Because of its slow water exchange, the SA isomer has been so far considered to be an undesired species and the ligands forming such complexes have been omitted in the search for high-efficiency CAs.

In this work, we investigate in detail the Ln^{III} complexes of a previously reported[13] a pyridine-*N*-oxide derivative of DOTA, $H_3do3apy^{NO}$ ($H_3\mathbf{L^1}$, 10-[(1-oxidopyridin-2-yl)-methyl]-1,4,7,10-tetraazacyclododecane-1,4,7-triacetic acid), and of its new bifunctional derivative $H_4do3apy^{NO-C}$ ($H_4\mathbf{L^2}$, 10-[(4-carboxy-1-oxidopyridin-2-yl)methyl]-1,4,7,10-tetraaza-cyclododecane-1,4,7-triacetic acid) (Chart 1), which bears an additional carboxylic group on the pyridine moiety. The pyridine-*N*-oxide pendant arm creates a six-membered chelate ring after coordination to the Ln^{III} ions, and such steric demands result in acceleration of the water exchange in the Gd^{III} complexes to a nearly optimal value. The syntheses of the ligands and relaxometric properties of the Gd^{III} complexes are reported in an accompanying paper.[14] Here we focus on the coordinating aspects of the six-membered chelate ring and its impact on the isomerism of the Ln^{III} complexes. The structures of the Ln^{III} complexes were investigated by X-ray diffraction in the solid state and by UV−vis and NMR spectroscopy in solution.

Experimental Section

Preparation of the Ln^{III} Complexes. The synthesis of the ligands $H_3\mathbf{L^1}$ and $H_4\mathbf{L^2}$ is described in an accompanying paper.[14] The Ln^{III} complexes of $H_3\mathbf{L^1}$ were prepared by mixing the ligand with 1.1 equiv of lanthanide(III) chloride in a small amount of distilled water, adjusting to pH 7 with 2 M KOH, and stirring overnight at room temperature. The inorganic salts including the excessive Ln^{III} ions were removed on Amberlite XAD-1180 by elution with distilled water, and a pure complex was released from the column with 20% aqueous EtOH. Evaporation of the solvents afforded the complexes as solid glassy materials with yields typically of about 75%. The complexes of $H_4\mathbf{L^2}$ were prepared alternatively with 10% excess of the ligand and purified subsequently on an Amberlite CG50 ion-exchange resin with water elution. The excessive ligand and most of the inorganic salts eluted in early fractions. The following fractions containing a pure complex were collected and combined. No chloride anions could be detected with $AgNO_3$ in the resulting solutions. In this procedure, the complexes were received as monoacids with a protonated carboxylic group on the pyridine ring. The pH was adjusted to 7 with LiOH and the solvent evaporated on a rotary evaporator to yield the complexes as glassy materials with yields typically of about 85%. All samples were checked using the xylenol orange test (urotropine buffer, pH 5.0) to exclude the presence of free Ln^{III} ions. The complexes were characterized by ^1H NMR, mass spectroscopy (MS), and reversed-phase high-performance liquid chromatography (HPLC). In all cases, the observed molecular peaks in MS were in accordance with the predicted masses and the general appearance of the spectra reflected the theoretical isotopic distribution of the lanthanides (Table S1 in the Supporting Information). The purities of the prepared complexes were assessed on HPLC and were greater than 98.7% in all cases (Table S2 and Figure S12 in the Supporting Information).

HPLC. The Ln^{III} complexes of $H_3\mathbf{L^1}$ and $H_4\mathbf{L^2}$ were analyzed on column Luna phenyl−hexyl 150 × 4.6 mm (Phenomenex) using isocratic elution with composition 5:95 (CH_3CN/H_2O with 0.1% trifluoroacetic acid), with detection at 254 nm (complexes of $H_3\mathbf{L^1}$) and 289 nm (complexes of $H_4\mathbf{L^2}$). The flow rates were maintained at 1 mL min^{-1}.

Single-Crystal Preparation. The single crystals of $[Tm(\mathbf{L^1})]\cdot 3H_2O$ and $[Yb(\mathbf{L^1})]\cdot 4H_2O$ were prepared from concentrated aqueous solutions of the complexes by a slow diffusion of acetone vapor. Crystals of $[Nd(H_2O)(\mathbf{L^1})]\cdot KCl\cdot HCl\cdot 7.5H_2O$ were obtained from an unpurified complex solution by a slow diffusion of acetonitrile vapor.

X-ray Structure Determination. Selected crystals were mounted on a glass fiber in a random orientation and cooled to 150(1) K. The diffraction data were collected by employing a Nonius Kappa CCD diffractometer (Enraf-Nonius) using Mo Kα (λ = 0.710 73 Å) at 150(1) K (Cryostream Cooler Oxford Cryosystem) and analyzed using the *HKL DENZO* program package.[15] The structures were solved by direct methods and refined by full-matrix least-squares techniques (*SIR92*[16] and *SHELXL97*[17]). The used scattering factors for neutral atoms were included in the *SHELXL97* program. Selected experimental data are listed in Table 1.

In the structure of $[Nd(H_2O)(\mathbf{L^1})]\cdot KCl\cdot HCl\cdot 7.5H_2O$, all non-hydrogen atoms were refined anisotropically. The solvate water molecules were best refined in nine positions, six of them with full occupancy and the last three with half-occupancy, giving in total

(12) (a) Woods, M.; Aime, S.; Botta, M.; Howard, J. A. K.; Moloney, J. M.; Navet, M.; Parker, D.; Port, M.; Rousseaux, O. *J. Am. Chem. Soc.* **2000**, *122*, 9781–9792. (b) Woods, M.; Kovacs, Z.; Zhang, S. R.; Sherry, A. D. *Angew. Chem., Int. Ed.* **2003**, *42*, 5889–5892. (c) Woods, M.; Botta, M.; Avedano, S.; Wang, J.; Sherry, A. D. *Dalton Trans.* **2005**, 3829–3837.
(13) Polášek, M.; Rudovský, J.; Hermann, P.; Lukeš, I.; Vander Elst, L.; Muller, R. N. *Chem. Commun.* **2004**, 2602–2603.
(14) Polášek, M.; Šedinová, M.; Kotek, J.; Vander Elst, L.; Muller, R. N.; Hermann, P.; Lukeš, I. *Inorg. Chem.* **2009**, *48*, 455−465.
(15) (a) Otwinovski, Z; Minor, W. *HKL Denzo and Scalepack Program Package*; Nonius BV: Delft, The Netherlands, 1997; (b) Otwinovski, Z.; Minor, W. *Methods Enzymol.* **1997**, *276*, 307–326.
(16) Altomare, A.; Burla, M. C.; Camalli, M.; Cascarano, G.; Giacovazzo, C.; Guagliardi, A.; Polidori, G. *J. Appl. Crystallogr.* **1994**, *27*, 435–435.
(17) Sheldrick, G. M. *SHELXL97, A Computer Program for Refinement of Crystal Structures*; University of Göttingen: Göttingen, Germany, 1997.

Table 1. Experimental Data of Reported Crystal Structures

parameters	$[Nd(H_2O)(\mathbf{L^1})]\cdot KCl\cdot HCl\cdot 7.5H_2O$	$[Tm(\mathbf{L^1})]\cdot 3H_2O$	$[Yb(\mathbf{L^1})]\cdot 4H_2O$
formula	$C_{20}H_{46}Cl_2KN_5NdO_{15.5}$	$C_{20}H_{34}N_5O_{10}Tm$	$C_{20}H_{36}N_5O_{11}Yb$
M	858.86	673.45	695.58
color, shape	colorless, needle	colorless, prism	colorless, needle
crystal system	triclinic	triclinic	monoclinic
space group	$P\bar{1}$ (No. 2)	$P\bar{1}$ (No. 2)	$P2_1/n$ (No. 14)
a/Å	9.1639(2)	7.31450(10)	10.3419(2)
b/Å	12.5348(4)	10.6758(3)	7.47780(10)
c/Å	16.6075(6)	15.7482(4)	33.3682(5)
α/deg	68.9110(14)	81.7654(12)	90.00
β/deg	76.426(2)	86.6648(15)	95.5528(8)
γ/deg	87.844(2)	89.6355(16)	90.00
U/Å^3	1727.87(9)	1215.01(5)	2568.41(7)
Z	2	2	4
D_c/g cm^{-3}	1.651	1.841	1.799
μ/mm^{-1}	1.848	3.716	3.708
$R1$ [$I \geq 2\sigma(I)$]; $R2$ (all data)[a]	0.0354; 0.0457	0.0299; 0.0311	0.0272; 0.0379
$wR1$ [$I \geq 2\sigma(I)$]; $wR2$ (all data)[a]	0.0843; 0.0895	0.0727; 0.0732	0.0588; 0.0634

[a] $R1$, $R2 = \sum|F_o - F_c|/\sum|F_c|$; $wR1$, $wR2 = [\sum w(F_o^2 - F_c^2)^2/\sum w(F_o^2)^2]^{1/2}$.[17]

7.5 molecules. The hydrogen atoms, including those attached to water oxygen atoms, were located using the electron density difference map; however, they were fixed in theoretical (C−H) or original (O−H) positions using $U_{eq}(H) = 1.2U_{eq}(X)$. The HCl proton necessary to reach electroneutrality of the crystal was not located (see CCDC-710314).

In the structure of $[Tm(\mathbf{L^1})]\cdot 3H_2O$, all non-hydrogen atoms were refined anisotropically. Two solvate water molecules were refined with full occupancy, and the last one was disordered in three positions with a relative occupancy of 40:40:20 (% fixed). All hydrogen atoms (including those attached to water oxygen atoms) were located in the electron density difference map, except for those attached to the disordered solvate water molecule. To keep a low number of parameters, they were fixed in theoretical (C−H) or original (O−H) positions using $U_{eq}(H) = 1.2U_{eq}(X)$. Because of a high absorption coefficient, absorption correction (Gaussian integration)[18] with scaling factors $T_{min} = 0.214$ and $T_{max} = 0.608$ was applied (see CCDC-710315).

In the structure of $[Yb(\mathbf{L^1})]\cdot 4H_2O$, all non-hydrogen atoms were refined anisotropically. Three solvate water molecules were refined with full occupancy, and the last one was disordered in two positions with a relative occupancy of 52:48 (% refined). All hydrogen atoms (including those attached to water oxygen atoms and even the disordered solvate water molecule) were located in the electron density difference map. In the final cycles, hydrogen atoms were fixed in theoretical (C−H) or original (O−H) positions using $U_{eq}(H) = 1.2U_{eq}(X)$. Because of a high absorption coefficient, absorption correction (Gaussian integration)[18] with scaling factors $T_{min} = 0.489$ and $T_{max} = 0.800$ was applied (see CCDC-710316).

NMR Measurements. ^{1}H NMR spectra were acquired on a Varian UNITY INOVA 400. The temperature was controlled with an L-900 VT unit and calibrated on ^{1}H NMR signals of methanol.[19] The samples for low-temperature measurements were dissolved in a 4:1 mixture of CD_3OD (99.8%) and D_2O (99.95%) with 0.5% *t*-BuOH as a reference. The samples were maintained in the probe for at least 10 min before measurement to ensure temperature equilibration.

UV−Vis Measurements. UV−vis spectra of $^7F_0 \rightarrow {}^5D_0$ transitions of Eu^{III} complexes of $H_3\mathbf{L^1}$ were obtained on a Varian Cary 5000 spectrophotometer in the region 578−582 nm (17182−17300 cm^{-1}) with data intervals of 0.005 nm and an integration time of 10 s. The sample concentration was ∼0.06 M, and the spectra were measured in the temperature range 10−65 °C. Spectra were fitted by two contributing bands of shape given by a linear combination of Gaussian and Lorentzian functions.

Mass Spectrometry. Mass spectra were recorded on a Bruker ESQUIRE 3000 with electrospray ionization and ion-trap detection in positive (complexes of $H_3\mathbf{L^1}$) or negative (complexes of $H_4\mathbf{L^2}$) modes.

Results and Discussion

Crystal Structures. Single crystals were successfully prepared and analyzed by X-ray diffraction in the cases of Nd^{III}, Dy^{III},[13] Tm^{III} and Yb^{III} complexes of $H_3\mathbf{L^1}$. The diffraction analysis revealed the composition of the newly prepared crystals as $[Nd(H_2O)(\mathbf{L^1})]\cdot KCl\cdot HCl\cdot 7.5H_2O$, $[Tm(\mathbf{L^1})]\cdot 3H_2O$, and $[Yb(\mathbf{L^1})]\cdot 4H_2O$, respectively. No suitable crystals were obtained for the complexes of $H_4\mathbf{L^2}$.

In all cases, the anion $(\mathbf{L^1})^{3-}$ was found to be coordinated to the central ion in an octadentate fashion, with the pyridine-*N*-oxide pendant arm forming a six-membered chelate ring. The oxygen atom of the pyridine-*N*-oxide is bound only slightly above (0.12−0.24 Å) the plane defined by the remaining three oxygen atoms (O311, O411, and O511) and, thus, all coordinated oxygen atoms form a nearly perfect O_4 square. The N_4 and O_4 planes are almost parallel, sandwiching the metal ion. The relevant parameters of all discussed structures are listed in Tables 2 and S3 in the Supporting Information.

The configurations of the pendant arms and of the macrocyclic ring, $\Delta\lambda\lambda\lambda\lambda$ and $\Lambda\delta\delta\delta\delta$, unambiguously define the SA isomers in all cases. The torsion angles between the N_4 and O_4 planes vary from ∼−35° to ∼−39° (Table 2). The structures can be divided into two groups, one that contains the mutually isostructural Dy^{III} [13] and Tm^{III} (Figure 2) complexes and the very similar Yb^{III} complex (Figure S1 in the Supporting Information) and the other that contains only the Nd^{III} complex (Figure 3). The most noticeable difference between these groups comes from the coordination of a water molecule, which was found only in the structure of the Nd^{III} complex (Figure 3). Thus, the coordination sphere found in this compound adopts a monocapped SA structure, with the water molecule in the capping position. The O1−Nd

(18) Coppens, P. In *Crystallographic Computing*; Ahmed, F. R., Hall, S. R., Huber, C. P., Eds.; Munksgaard: Copenhagen, Denmark, 1970; pp 255−270.
(19) Bornais, J.; Brownstein, S. *J. Magn. Reson.* **1978**, *29*, 207–211.

Table 2. Selected Structural Parameters Found in Crystal Structures of the Complexes

	$[Nd(H_2O)(\mathbf{L^1})]\cdot KCl\cdot HCl\cdot 7.5H_2O$	$[Eu(H_2O)(\mathbf{L^5})](CF_3SO_3)_2$[a,22]	$[Dy(\mathbf{L^1})]\cdot 3H_2O$[13]	$[Tm(\mathbf{L^1})]\cdot 3H_2O$	$[Yb(\mathbf{L^1})]\cdot 4H_2O$
conformation	*syn*-SA	*syn*-SA	*anti*-SA	*anti*-SA	*anti*-SA
		Distances (Å)			
d(Ln−O1)	2.506(3)	2.486			
d(N22−O22N)	1.334(4)		1.340(2)	1.338(4)	1.350(4)
d(Ln−O22N)	2.409(3)	2.242	2.319(2)	2.287(3)	2.305(2)
d(Ln−O311)	2.435(3)	2.387	2.278(2)	2.248(3)	2.235(2)
d(Ln−O411)	2.413(3)	2.403	2.308(1)	2.277(3)	2.254(2)
d(Ln−O511)	2.397(3)	2.383	2.281(2)	2.250(3)	2.243(2)
d(Ln−N1)	2.706(4)	2.643	2.598(2)	2.566(3)	2.542(3)
d(Ln−N4)	2.669(4)	2.677	2.574(2)	2.544(3)	2.520(3)
d(Ln−N7)	2.681(4)	2.745	2.585(2)	2.551(3)	2.536(3)
d(Ln−N10)	2.692(4)	2.685	2.578(2)	2.543(3)	2.526(3)
d(Ln−OQ)[b]	0.763	0.785	1.005	1.022	1.026
d(Ln−NQ)[b]	1.656	1.644	1.500	1.462	1.425
d(NQ−OQ)[b]	2.418	2.420	2.503	2.482	2.451
d(arom−N1)[c]	1.083(6)	1.174	1.023(3)	1.017(5)	1.049(4)
d(arom−Ln)[c]	1.118(5)	1.199	2.055(2)	2.037(3)	2.080(3)
d(H231−Ln)	4.69	4.59	4.18	4.25	4.19
		Angles (deg)			
∠(H231−Ln−OQ)[b]	68.0	71.1	37.7	36.1	34.7
∠(N_4−O_4)	5.2(2)	4.5	5.6(1)	5.1(1)	4.5(1)
∠(O22N−Ln−O411)	139.9(1)	136.0	125.0(1)	123.7(1)	124.7(1)
∠(O311−Ln−O511)	146.3(1)	146.0	131.1(1)	128.9(1)	127.2(1)
∠(arom−O_4)[c]	47.2(1)	46.2	86.34(5)	86.21(9)	86.15(7)
		Torsion Angles (deg)			
∠(O22N−OQ−NQ−N1)[b]	−37.6	−37.5	−32.3	−33.7	−36.2
∠(O311−OQ−NQ−N4)[b]	−39.8	−38.5	−36.7	−37.4	−37.8
∠(O411−OQ−NQ−N7)[b]	−39.0	−37.2	−36.6	−37.5	−39.2
∠(O511−OQ−NQ−N10)[b]	−37.3	−36.7	−35.0	−35.9	−37.3

[a] Atoms were arbitrarily renumbered according to our numbering scheme. [b] OQ and NQ are centroids (centers of gravity) of O_4 (O22N, O311, O411, and O511) and N_4 (N1, N4, N7, and N10) planes, respectively. [c] "arom" stands for the plane defined by the pyridine-*N*-oxide pendant arm (O22N, N22, C23, C24, C25, C26, C21, and C20 atoms).

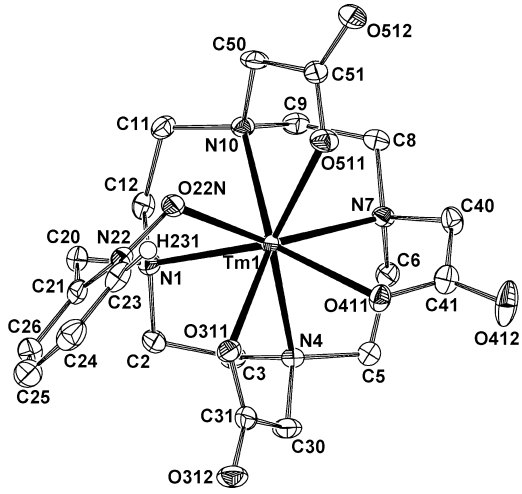

Figure 2. Molecular structure of the *anti*-SA $[Tm(\mathbf{L^1})]$ complex molecule ($\Lambda\delta\delta\delta\delta$ isomer) found in the crystal structure of $[Tm(\mathbf{L^1})]\cdot 3H_2O$. Hydrogen atoms (except for H231) are omitted for the sake of clarity.

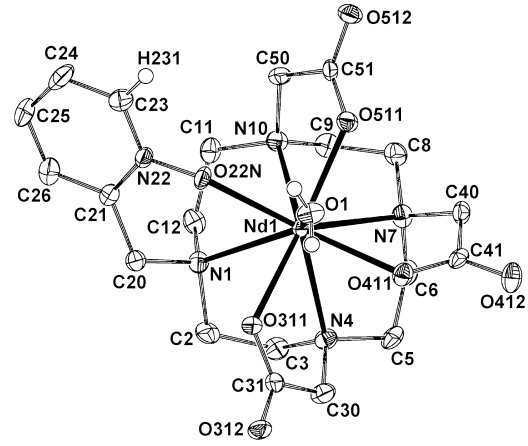

Figure 3. Molecular structure of the *syn*-SA $[Nd(H_2O)(\mathbf{L^1})]$ complex molecule ($\Lambda\delta\delta\delta\delta$ isomer) found in the crystal structure of $[Nd(H_2O)(\mathbf{L^1})]\cdot KCl\cdot HCl\cdot 7.5H_2O$. Hydrogen atoms (except for H231 and those of water) are omitted for the sake of clarity.

distance (2.506 Å) is almost the same as that in the reported structure of $[Nd(H_2O)(dota)]^-$ (2.508 Å).[20] The Nd^{III} ion is placed close to the O_4 plane (0.76 Å), which results in wide transangular ("opening") angles of 140° and 146° (O22N−Nd−O411 and O311−Nd−O511 angles, respectively) and, consequently, creates enough space for one water molecule to occupy the ninth coordinating position.[21] The molecular structure of the complex is very similar to that found in the solid-state structure of $[Eu(H_2O)(\mathbf{L^5})](CF_3SO_3)_2$ reported previously (Chart 1).[22] Contrary to these structures, the central ions in the structures of Dy^{III}, Tm^{III}, and Yb^{III} complexes are farther from the O_4 plane (∼1.02 Å). This reduces the "opening" angles to the range 124−131° (Table 2) and prevents the water molecule from coordination.

(20) Benetollo, F.; Bombieri, G.; Calabi, L.; Aime, S.; Botta, M. *Inorg. Chem.* **2003**, *42*, 148–157.

(21) (a) Lukeš, I.; Kotek, J.; Vojtíšek, P.; Hermann, P. *Coord. Chem. Rev.* **2001**, *216−217*, 287–312. (b) Hermann, P.; Kotek, J.; Kubíček, V.; Lukeš, I. *Dalton Trans.* **2008**, 3027–3047. (c) Vojtíšek, P.; Cígler, P.; Kotek, J.; Rudovský, J.; Hermann, P.; Lukeš, I. *Inorg. Chem.* **2005**, *44*, 5591−5599. (d) Kotek, J.; Rudovský, J.; Hermann, P.; Lukeš, I. *Inorg. Chem* **2006**, *45*, 3097–3102.

Distances of the central ions from the N_4 plane change from 1.66 Å for the larger Nd^{III} ion to 1.43 Å for the smaller Yb^{III} ion and follow the expected trend.[21] The bond lengths of the *N*-oxide (N22−O22N) bonds in the complexes (Table 2) are not significantly changed in comparison with that of the free ligand (1.34 Å).[14] This is in accordance with the expected strong ionic character of the coordination bond.

The two groups of structures differ in the conformation of the coordinated pyridine-*N*-oxide arm. The orientation follows the direction of rotation of the acetate arms in the Nd^{III} complex; an analogous situation was also observed in the structure of the $[Eu(H_2O)(\mathbf{L^5})]^{2+}$ complex.[22] However, in the other structures, only the methylene group bearing the pyridine moiety is turned in the direction of the acetates and the pyridine ring itself is bent backward. In the following text, we will use the symbols *syn*-SA (pyridine in the direction of the acetates) and *anti*-SA (pyridine opposite to the acetates) to discriminate between the two conformers. These two arrangements reflect the conformational flexibility of the six-membered chelate ring. The difference between these two arrangements becomes apparent when the distances of N1 and Ln^{III} from the plane defined by the aromatic pendant arm are compared (Table 2). Thus, the chelate ring, although strongly distorted, can be viewed to be in the boat [d(pyN^{ox}−N1) and d(pyN^{ox}−Ln) are approximately equal, ∼1.1 Å] and twisted-boat [d(pyN^{ox}−N1) ∼ 1.0 Å and d(pyN^{ox}−Ln) ∼ 2.1 Å] conformations (Figure S3 in the Supporting Information). A boatlike conformation found in the $[Nd(H_2O)(\mathbf{L^1})]$ and $[Eu(H_2O)(\mathbf{L^5})]^{2+}$ [22] complexes turns the aromatic pendant arm to the direction of the acetate rotation (*syn*-SA), while a twisted-boat-like conformation in the other complexes forces the opposite arrangement (*anti*-SA). Both conformers significantly differ also in the angle between the plane of the aromatic pendant arm (arom plane) and coordinated oxygen atoms (O_4 plane). In the *syn*-SA arrangement (the Nd^{III} and Eu^{III} complexes), the angle is ∼46°, while the planes are mutually perpendicular in the *anti*-SA conformation found in the Dy^{III}, Tm^{III}, and Yb^{III} complexes (Table 2). Such conformation flexibility also leads to a significant difference in the position of hydrogen atom H231 (hydrogen atom in the α position to the pyridine nitrogen atom; see Figures 2 and 3) with respect to the magnetic axis of the complexes (direction of the pseudo-C_4 axis, approximated by the Ln−OQ vector, where OQ represents the center of gravity of the O_4 plane). In the *syn*-SA arrangement, the distance of the atom H231 from the metal center is ∼4.6−4.7 Å, and the angle between the Ln−H321 vector and the magnetic axis is ∼70°. However, in the *anti*-SA arrangement, this atom is somewhat closer to the metal ion (∼4.2 Å) and the corresponding angle (∼35−38°) is much smaller than the "magic" angle defining the McConnell cone (54.7°). Such positions significantly influence the ^{1}H NMR spectra (see below).

(22) Woods, M.; Kiefer, G. E.; Bott, S.; Castillo-Muzquiz, A.; Eshelbrenner, C.; Michaudet, L.; McMillan, K.; Mudigunda, S. D. K.; Ogrin, D.; Tircso, G.; Zhang, S.; Zhao, P.; Sherry, A. D. *J. Am. Chem. Soc.* **2004**, *126*, 9248–9256.

The exact position of the pyridine-*N*-oxide pendant arm has a large effect on the distances between the N_4 and O_4 planes. In general, these distances are larger in the complexes of $H_2\mathbf{L^1}$ than in the corresponding SA structures found in complexes of DOTA (Nd^{III} = 2.418 Å for $H_3\mathbf{L^1}$ vs 2.360 Å for DOTA;[20] Dy^{III} = 2.503 Å for $H_3\mathbf{L^1}$ vs 2.340 Å for DOTA[20]). Coordination of the pyridine-*N*-oxide arm thus apparently expands the cavity of the ligand. This effect is more apparent in the case of *anti*-SA structures found in the Dy^{III}, Tm^{III}, and Yb^{III} complexes (see Table 2). Because of the *anti*-SA arrangement, the distances between the N_4 and O_4 planes are larger for the heavier lanthanides than for the Nd^{III} complex with the *syn*-SA arrangement, despite the decreasing ionic radii. In this respect, the *anti*-SA structures are close to the TSA structures found in some complexes of DOTA, which show similarly large distances of the planes (compare 2.482 Å in *anti*-SA-[Tm($\mathbf{L^1}$)] and 2.530 Å in TSA-$[Tm(dota)]^-$ [20]).

In the structure of $[Nd(H_2O)(\mathbf{L^1})]\cdot KCl\cdot HCl\cdot 7.5H_2O$, the $[Nd(H_2O)(\mathbf{L^1})]$ molecules are joined through coordination of carboxylate oxygen atoms to potassium into double chains, which lie in the planes. Water molecules and chloride anions are placed between these planes and form an extensive hydrogen-bond network (Figure S2 in the Supporting Information). The complex molecules in the structures of $[Tm(\mathbf{L^1})]\cdot 3H_2O$ and $[Yb(\mathbf{L^1})]\cdot 4H_2O$ are connected via hydrogen bonds with solvate water molecules.

Solution Structures of Ln^{III} Complexes. It is essential for the function of a Gd^{III}-based MRI CA that a water molecule is coordinated to the central ion. However, no coordinated water molecule was found in the X-ray structures of the Dy^{III}, Tm^{III}, and Yb^{III} complexes of $H_3\mathbf{L^1}$, even though inner-sphere water was found in the Eu^{III} and Dy^{III} complexes of both ligands studied in solution.[13,14] In this respect, the solid-state structures do not reflect the structures of the complexes in solution. The solution structures must be, on average, more open or the Ln^{III} ions situated closer to the O_4 plane, so that the structures are more accessible for coordination of water. The same structural demands of the pyridine-*N*-oxide that accelerate the water exchange in the Gd^{III} complexes in solution prevent water from coordination in the solid state.

In determining the isomerism of the complexes in solution, we have focused mainly on the complexes of $H_3\mathbf{L^1}$ because the properties observed in NMR and optical absorption spectra could be directly related to the solid-state structures. Because no solid-state structures were obtained for the complexes of $H_4\mathbf{L^2}$, these were examined only by a comparison of the NMR spectra with those of the complexes of $H_3\mathbf{L^1}$. Because of C_1 symmetry, the complexes give very complicated NMR spectra and only the signals most relevant to isomerism could be identified (axial protons and H231, see below). However, examination of these signals and a comparison between the complexes of $H_3\mathbf{L^1}$ and $H_4\mathbf{L^2}$ led to the same conclusions regarding isomerism and dynamics. No evidence was noticed that the carboxylate on the pyridine ring in $H_4\mathbf{L^2}$ could coordinate to the central ion or signifi-

cantly affect the structure of the complexes in any way. All ^{1}H NMR spectra of the studied complexes are shown in the Supporting Information.

The isomerism of the Ln^{III} complexes of DOTA-like ligands has an important impact on the water exchange rate. Generally, the TSA isomer exchanges the coordinated water molecule faster and is therefore preferred to the SA isomer in the search for more efficient CAs.[11,12] Having observed a fast water exchange on the Gd^{III} complexes of $H_3\mathbf{L^1}$ and $H_4\mathbf{L^2}$,[13,14] we decided to explore the TSA/SA isomerism of the Ln^{III} complexes of these ligands in solution. A large sensitivity of the lanthanide-induced-shift (LIS) effect to structural changes makes the measurement of ^{1}H NMR spectra an excellent method to evaluate this isomerism.[10,12,23] The axial protons of the macrocyclic ring (Figure S4 in the Supporting Information) usually show the strongest LIS effect and, therefore, are shifted away from the other signals in the spectrum.[10,12,23] Values of the shift differ significantly for both diastereomers yet remain comparable for complexes of various DOTA-like ligands of the same stereochemistry.[10,12] High-resolution NMR measurements of Gd^{III} complexes are not feasible because of the extremely fast-induced relaxation, but one can investigate the other Ln^{III} ions and extrapolate the properties to the Gd^{III} complex itself.[10b] To study the isomerism in solution, we have focused on the Nd^{III}, Eu^{III}, and Yb^{III} complexes because they are good representatives of the whole lanthanide series and provide lucid ^{1}H NMR spectra. The Eu^{III} complexes were examined in greater detail because they are structurally closest to the Gd^{III} complexes and allow measurements of both the NMR and optical absorption spectra.

The signals of the axial protons appear in the low-field region in the spectra of the Eu^{III} and Yb^{III} complexes and in the high-field region in the Nd^{III} complexes (Figures 4 and S5−S7 in the Supporting Information). In all cases, only one set of these signals was detected at 25 °C, thus indicating the presence of only one of the isomers. For example, in the case of the Eu^{III} complex, the signals appear in the interval from 37 to 28 ppm (Figure 4), a region typical for the signals of SA isomers.[10,12] Similarly, the NMR spectra could be ascribed only to SA isomers also in the cases of the Nd^{III} and Yb^{III} complexes (Figures S5 and S6 in the Supporting Information). However, when the spectrum of the Eu^{III} complex was recorded at −35 °C in a CD_3OD/D_2O (4:1) mixture, a new set of signals emerged in the region characteristic for the TSA isomer (Figure 4). The ratio of the isomers, estimated from the integral intensities after deconvolution of the peaks, is approximately 45:1 in favor of the SA isomer. This corresponds to only 2% of the TSA isomer in the mixture. Similarly, a low abundance of TSA was found in the Nd^{III} complex at temperatures below −35 °C, but no TSA was detected in the Yb^{III} complex even at −47 °C (Figures S5 and S6 in the Supporting Information). With increasing temperature, the ^{1}H NMR signals of the TSA isomer of the Eu^{III} complex become broader and less

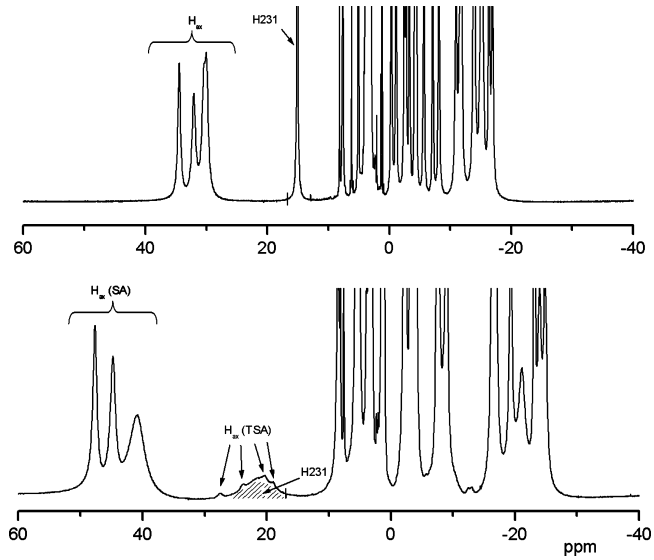

Figure 4. ^{1}H NMR spectra of $[Eu(H_2O)(\mathbf{L^1})]$ in a CD_3OD/D_2O mixture (4:1) at 25 (top) and −35 °C (bottom). H_{ax} denotes the signals of the axial protons (see Figure S4 in the Supporting Information for the definition of H_{ax}).

intensive, until coalescence with the signals of the SA isomer is reached around −20 °C (Figure 5). This points to an unusually fast exchange process between the two isomers. Because of the low temperature of coalescence and a low intensity of the signals, we did not observe the TSA isomer in our previous work.[13]

From a molecular dynamics point of view, the presence of only one isomer in solution at room temperature brings two possibilities. Either the enantiomers of this isomer interconvert through simultaneous inversion of the macrocycle and rotation of the pendant arms or the enantiomerization is halted. We have qualitatively examined the dynamics of the Eu^{III} complex (Figure S8 in the Supporting Information) of $H_3\mathbf{L^1}$ by the ^{1}H NMR EXSY (EXchange SpectroscopY) experiment. The enantiomerization $\Delta\lambda\lambda\lambda\lambda \leftrightarrow \Lambda\delta\delta\delta\delta$ was confirmed by the presence of single cross-peaks for all signals in the spectrum, except for the protons of the pyridine-*N*-oxide, which do not change their environments during the process. However, the observation of the TSA isomer at low temperatures means that the inversion of the macrocycle and rotation of the pendant arms do not occur simultaneously. Therefore, the enantiomerization of the SA isomer is mediated through the TSA isomer as well as in complexes of DOTA (see Figure 1).[10] However, in our case, the TSA configuration should be considered as an unstable intermediate rather than an isomer.

The effect of the pyridine-*N*-oxide pendant on the isomerism of the Ln^{III} complexes can be further investigated by a comparison with similar compounds. Unfortunately, only a few derivatives of DOTA that also form a six-membered chelate ring by coordination of the pendant arm have been synthesized, and the isomerism of their Ln^{III} complexes has been studied only marginally. The ligand $H_3\mathbf{L^3}$ (Chart 1), which contains a pyridine pendant arm and thus forms a five-membered chelate ring, gives a mixture of isomers in the Eu^{III} complex with a TSA/SA ratio of about 1:2.[24] The complexes of nitrophenolic derivatives $H_4\mathbf{L^4}$ and $H\mathbf{L^5}$ (Chart

(23) Marques, M. P. M.; Geraldes, C. F. G. C.; Sherry, A. D.; Merbach, A. E.; Powell, H.; Pubanz, D.; Aime, S.; Botta, M. *J. Alloys Compnd.* **1995**, *225*, 303–307.

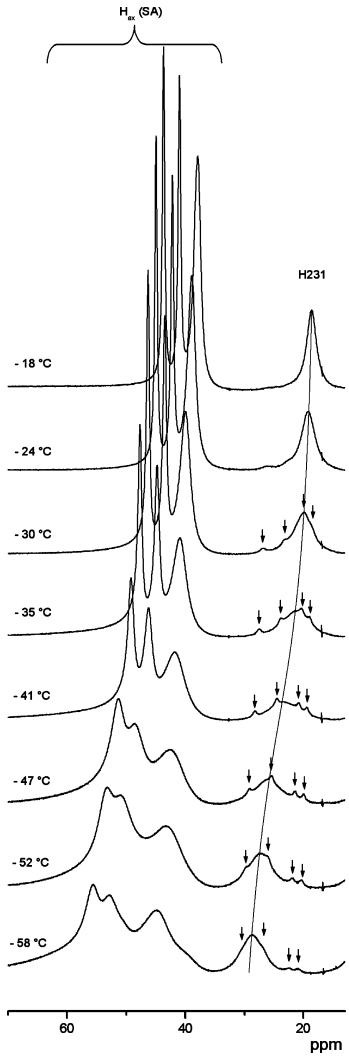

Figure 5. Low-field region of the ^{1}H NMR spectrum of [Eu(H$_2$O)(**L^1**)] in a CD$_3$OD/D$_2$O mixture (4:1) as a function of the temperature: signals of the axial protons of the SA isomer are labeled as H$_{ax}$ (SA); axial protons of the TSA isomer are labeled with arrows; the solid line tracks the position of the H231 signal. For the definition of the labeling scheme, see Figure S4 in the Supporting Information (H$_{ax}$ protons) and Figures 2 and 3 (H231).

1), which are structurally very close to our pyridine-*N*-oxide derivatives, were not studied from this point of view.[22] However, the published ^{1}H NMR spectra of their Eu^{III} complexes show several resemblances to our compounds. The first similarity is that, although the acid H$_4$**L^4** affords a mixture of isomers of the Eu^{III} complex, the SA structure largely predominates. The triamide H**L^5** gives only one set of broadened signals of the SA isomer, probably because of a fast isomerization. In this respect, it greatly resembles the properties of H$_3$**L^1** and H$_4$**L^2**. From a comparison of the above-mentioned compounds, we assume that the presence of a six-membered chelate ring, formed by coordination of a pendant arm, destabilizes the TSA structure of the complexes, resulting in suppression of the TSA isomer in solution and acceleration of the isomerization process between the TSA and SA isomers. However, more of such compounds would have to be examined to comprehend this trend properly. Unfortunately, no information about the isomerism of the complexes of a monopropionate derivative of DOTA and its phosphonate analogue, H$_4$**L^6** and H$_5$**L^7** (Chart 1), was provided.[8,25] The derivative **L^8** (Chart 1), which contains four 2-carbamoylethyl pendant arms capable of forming six-membered chelate rings, does not form stable Ln^{III} complexes in aqueous solutions.[26] However, the SA isomer was identified in the solid-state structure of the La^{III} complex of **L^8**.[26] An introduction of two 1,7-positioned pyridine-*N*-oxide units to the structure of DOTA[27] results in the same "absolute" preference of the ligand for the SA isomer as that found in the cases of H$_3$**L^1** and H$_4$**L^2**. Two such derivatives, H**L^9** and **L^{10}** (Chart 1), have been recently synthesized and their Yb^{III} complexes covalently bound to a model protein as paramagnetic NMR shift probes. The presence of only one isomer greatly simplified the two-dimensional NMR spectra of the protein. The ease of the synthesis is a clear advantage of the pyridine-*N*-oxide derivatives and provides an efficient method to a pure SA isomer.

To supplement the information obtained by NMR spectroscopy, we have investigated the Eu^{III} complex of H$_3$**L^1** by optical absorption measurements over the temperature range from 10 to 65 °C. Because the ^{5}D$_0$ and ^{7}F$_0$ states of Eu^{III} are nondegenerate, no crystal-field fine structure is expected for the ^{7}F$_0$ → ^{5}D$_0$ line. The number of bands observed for this transition is a measure of the number of crystallographically nonequivalent sites in the solid Eu^{III} compounds or for the number of Eu^{III}-containing species in solution. However, the ^{7}F$_0$ → ^{5}D$_0$ line is allowed in a selected number of symmetries only (C_{nv}, C_n, and C_s).[28] A detailed analysis of the absorption spectra in the region of the ^{7}F$_0$ → ^{5}D$_0$ transition can provide insight into the structure and dynamics of the Eu^{III} complexes because the transition energy is sensitive to the number and nature of the coordinated atoms as well as to the coordination geometry of the central Eu^{III} ion.[29] The shape of the ^{7}F$_0$ → ^{5}D$_0$ absorption band around 580 nm (17 241 cm^{-1}) found in the spectrum of [Eu(H$_2$O)(**L^1**)] displayed some asymmetry, and a satisfactory fit of the data was obtained only when two components were taken into account (Figures 6 and S9 in the Supporting Information). The band at lower energy (band A) appeared to be more intense than the band at higher energy (band B). Two bands are commonly observed when a hydration equilibrium or TSA/SA isomerism is involved in the systems.[30,31] These two cases can be distinguished according

(24) Aime, S.; Batsanov, A. S.; Botta, M.; Howard, J. A. K.; Lowe, M. P.; Parker, D. *New J. Chem.* **1999**, *23*, 669–670.

(25) Mamedov, I.; Mishra, A.; Angelovski, G.; Mayer, H. A.; Palsson, L.-O.; Parker, D.; Logothetis, N. K. *Dalton Trans.* **2007**, 5260–5267.

(26) Morrow, J. R.; Amin, S.; Lake, C. H.; Churchill, M. R. *Inorg. Chem.* **1993**, *32*, 4566–4572.

(27) (a) Keizers, P. H. J.; Desreux, J. F.; Overhand, M.; Ubbink, M. *J. Am. Chem. Soc.* **2007**, *129*, 9292–9293; (b) Keizers, P. H. J.; Saragliadis, A.; Hiruma, Y.; Overhand, M.; Ubbink, M. *J. Am. Chem. Soc.* **2008**, *130*, 14802–14812.

(28) Binnemans, K. *Bull. Soc. Chim. Belg.* **1996**, *105*, 793–798.

(29) (a) Albin, M.; Horrocks, W. D., Jr. *Inorg. Chem.* **1985**, *24*, 895–900. (b) Horrocks, W. D., Jr.; Sudnick, D. R. *Acc. Chem. Res.* **1981**, *14*, 384–392. (c) Amin, S.; Voss, D. A., Jr.; Horrocks, W. D., Jr.; Lake, C. H.; Churchill, M. R.; Morrow, J. R. *Inorg. Chem.* **1995**, *34*, 3294–3300.

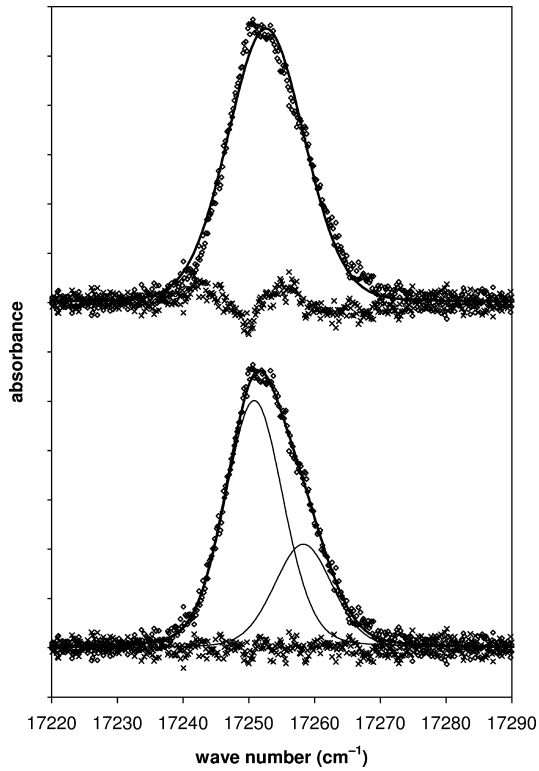

Figure 6. Representative absorption spectra of the $^7F_0 \rightarrow {}^5D_0$ transition of the [Eu(H_2O)($\mathbf{L^1}$)] complex measured at 25.3 °C. Comparison of the fitting with one band (upper) and two bands (lower). The measured data (diamonds) are shown with residual errors (crosses).

to the separation of the bands. For differently hydrated species, this value is about 0.5 nm (14.9 cm^{-1}) or larger.[30] However, the separation of 0.24 nm (7.1 cm^{-1}) observed in our case is closer to the values observed for mixtures of TSA/SA isomers.[31] The ratio of the integral intensities of the bands has been plotted as a function of the temperature, and the thermodynamic parameters of the equilibrium were assigned as follows: $\Delta H^0 = -8.6$ kJ mol^{-1}, $\Delta S^0 = 22$ J mol^{-1} K^{-1}, and $K_{B/A}{}^{298} = 0.443$ (Figure S10 in the Supporting Information). Although it suggests itself to relate the pair of bands A/B to the pair SA/TSA, there is a certain discrepancy between the optical absorption and NMR spectra that cannot be explained only by SA/TSA isomerism. First, because the signals of the isomers in the NMR spectrum at 298 K are averaged as a result of fast isomerization, the positions of the signals are weighted averages of the signals of separate isomers. A given ratio $K_{B/A}{}^{298} = K_{TSA/SA}{}^{298} = 0.443$ would lead to a noticeable shift of the signals of the axial protons toward the range typical for the TSA isomer. However, this is not the case, and the signals fit rather well to the SA region,[10,12,23] showing that the contribution of the TSA isomer is negligible. Second, with the thermodynamic parameters mentioned above, we could calculate the ratio of the species at −35 °C (238 K) as 84:16 (A/B), which is in stark contrast to the 98:2 mixture of the SA and TSA isomers determined from the ^{1}H NMR spectrum at the same temperature. For that reason, we assume that another type of isomerism other than TSA/SA has to be involved in the complex. The two different orientations (*syn*-SA/*anti*-SA) of the pyridine-*N*-oxide pendant arm found in the X-ray structures bring such a possibility (see above). To test this hypothesis, we traced the NMR signal of the aromatic proton neighboring the *N*-oxide group (proton H231; Figures 2, 3, and S1 in the Supporting Information) in the [Eu(H_2O)($\mathbf{L^1}$)] complex at low temperatures (Figure 5). This proton is located in the complex close to the central ion but is separated from it by four bonds. We can therefore assume that the resulting LIS effect is mainly realized by pseudocontact (i.e., through-space) interaction rather than by contact (i.e., through-bond) interaction.[32] The signal of H231 should therefore well reflect any changes in the position of the pyridine ring. This signal displays a sharp shape at 25 °C (Figure 4), showing that the exchange between the *syn*-SA and *anti*-SA isomers (if present) is fast compared to the NMR time scale. Being situated at 15 ppm, it experiences a strong positive LIS effect, which signifies that the average location of the proton is within the McConnell cone. Taking into account this induced shift and considering the two limiting positions found for H231 in the X-ray structures, we assume that the *anti*-SA isomer must be predominant in solution (compare Figures 2 and 3; see also Table 2). The signal broadens significantly with decreasing temperature and superimposes with the TSA axial protons below −20 °C. At −41 °C, it reaches the maximum width and begins to sharpen again below this temperature point (Figure S11 in the Supporting Information), while all of the other signals continue to broaden as a result of faster relaxation (Figure 5). This behavior suggests that a chemical exchange is involved in the broadening of this signal and that coalescence appears near −41 °C. Because the exchange between the SA and TSA structures has been "frozen" at −20 °C, the exchange observed on aromatic proton H231 must involve the pair *syn*-SA/*anti*-SA. The ^{1}H NMR signal of H231 found at −58 °C is situated at 28 ppm, and according to the strongly positive LIS effect, it can be assigned to the *anti*-SA isomer. Unfortunately, the NMR measurements at these low temperatures are complicated by extensive broadening and overlapping of the signals, troublesome baseline and phase corrections. Because of these difficulties, we could

(30) (a) Graeppi, N.; Powell, D. H.; Laurenczy, G.; Zekany, L.; Merbach, A. E. *Inorg. Chim. Acta* **1995**, *235*, 311–326. (b) Tóth, É.; Dhubhghaill, O. M. N.; Besson, G.; Helm, L.; Merbach, A. E. *Magn. Reson. Chem.* **1999**, *37*, 701–708. (c) Yerly, F.; Dunand, F. A.; Tóth, É.; Figueirinha, A.; Kovacs, Z.; Sherry, A. D.; Geraldes, C. F. G. C.; Merbach, A. E. *Eur. J. Inorg. Chem.* **2000**, 1001–1006. (d) Dunand, F. A.; Aime, S.; Geninatti, S. C.; Giovenzana, G. B.; Merbach, A. E. *Magn. Reson. Chem.* **2002**, *40*, 87–92. (e) Mato-Iglesias, M.; Platas-Iglesias, C.; Djanashvili, K.; Peters, J. A.; Tóth, É.; Balogh, E.; Muller, R. N.; Elst, L. V.; de Blas, A.; Rodriguez-Blas, T. *Chem. Commun.* **2005**, 4729–4731. (f) Balogh, E.; Mato-Iglesias, M.; Platas-Iglesias, C.; Tóth, É.; Djanashvili, K.; Peters, J. A.; de Blas, A.; Rodriguez-Blas, T. *Inorg. Chem.* **2006**, *45*, 8719–8728.

(31) (a) Amin, S.; Voss, D. A.; Horrocks, W. D., Jr.; Lake, C. H.; Churchill, M. R.; Morrow, J. R. *Inorg. Chem.* **1995**, *34*, 3294–3300. (b) Szilagyi, E.; Tóth, É.; Brücher, E.; Merbach, A. E. *J. Chem. Soc., Dalton Trans.* **1999**, 2481–2486. (c) Dunand, F. A.; Merbach, A. E. *Inorg. Chem. Commun.* **2001**, *4*, 719–722. (d) Muller, G.; Kean, S. D.; Parker, D.; Riehl, J. P. *J. Phys. Chem. A* **2002**, *106*, 12349–12355. (e) Costa, J.; Balogh, E.; Turcryl, V.; Tripier, R.; Le Baccon, M.; Chuburu, F.; Handel, H.; Helm, L.; Tóth, É.; Merbach, A. E. *Chem.—Eur. J.* **2006**, *12*, 6841–6851.

(32) Peters, J. A.; Huskens, J.; Raber, D. J. *Prog. Nucl. Magn. Reson. Spectrosc.* **1996**, *28*, 283–350.

not directly observe the corresponding H231 signal of the minor *syn*-SA isomer. To perform the NMR measurements at low temperatures, the complexes had to be dissolved in a nonfreezing CD_3OD/D_2O (4:1) mixture.[10a] The optical absorption measurements were, however, measured in pure H_2O. To test whether the solvents affect the isomerism, we have measured additional optical absorption spectra of $[Eu(H_2O)(\mathbf{L^1})]$ in a CH_3OH/H_2O (4:1) mixture. The ratio of the two bands was not altered and followed the same trend as that in H_2O (Figure S10 in the Supporting Information). Therefore, we conclude that the isomerism is not affected by the solvent.

The presence of two kinds of isomerism (SA/TSA and *syn/anti*) in one system theoretically allows the formation of four different isomers. The existence of the pair *syn*-SA/*anti*-SA is supported by X-ray structures, optical absorption, and NMR measurements. It is, in principle, possible that a pair of *syn*-TSA/*anti*-TSA is also present in solution. However, the low occurrence of the TSA isomer in solution did not allow investigations of this possibility. It thus remains unclear whether the TSA isomer observed in NMR spectra at low temperatures is *syn*-TSA or *anti*-TSA or a combination of both isomers in the fast exchange regime.

The low temperatures of coalescence observed in NMR spectra due to *syn*-SA/*anti*-SA isomerization (−41 °C) and SA/TSA isomerization (−20 °C) indicate that both processes have relatively low activation barriers. This can be expected for *syn*-SA/*anti*-SA exchange because it requires only a conformational change in a six-membered chelate ring. However, such a fast isomerization is unusual for the SA/TSA pair, and separate NMR signals are usually observed at temperatures above 0 °C for both isomers.[10,23,24] Similar, although not so pronounced, flexibility was noticed in the NMR spectra of Eu^{III} complexes of the nitrophenolic derivatives $H_4\mathbf{L^4}$ and $H\mathbf{L^5}$ (Supporting Information in ref 22). The introduction of a pendant arm capable of forming a six-membered chelate ring thus seems to enhance the flexibility of the coordination cage, which can easily switch between several different geometries. It is likely that this flexibility is also reflected in the water exchange. Indeed, there is a clear relationship between increasing the number of atoms in a chelate ring and accelerating the water exchange.[7−9] As a result, the water residence lifetimes found in $[Gd(H_2O)(\mathbf{L^1})]$ (39 ns) and $[Gd(H_2O)(\mathbf{L^2})]^-$ (34 ns) are almost optimal.[14] Interestingly, the thermodynamic and kinetic stabilities determined for Ln^{III} complexes of $H_3\mathbf{L^1}$ do not suffer from this increased flexibility; the values are between those found for complexes of DOTA and DO3A.[33]

Conclusion

The introduction of the pyridine-*N*-oxide pendant arm to the structure of DOTA leads to an unprecedented preference of the ligand to form the SA isomer in the Ln^{III} complexes. The six-membered chelate ring formed by coordination of pyridine-*N*-oxide greatly destabilizes the TSA arrangement, which exists only as an unstable intermediate during enantiomerization of the SA isomer. The use of the pyridine-*N*-oxide pendant arm thus provides a synthetically easy and efficient method to the single isomer. Derivatization of the pyridine-*N*-oxide in the 4 position had no significant effect on the isomerism of the complexes. Two conformations of the six-membered chelate ring were found in the solid state, resulting in parallel (*syn*-SA) or opposite (*anti*-SA) orientations of the pyridine ring relative to the rotation of the coordinated acetate arms. Such isomerism was observed for the first time in the Ln^{III} complexes of DOTA-like ligands. The UV−vis and NMR data suggest that these two forms are in dynamic equilibrium in solution. Investigations of solid-state structures revealed that coordination of the pyridine-*N*-oxide arm enlarges the cavity of the ligand in comparison with the complexes of DOTA. This increases the flexibility of the coordination cage in solution, which is reflected in the fast isomerization processes observed within the pairs of structures SA/TSA and *syn*-SA/*anti*-SA. The flexibility of the coordination cage in combination with the higher steric demands of the six-membered chelate ring are most likely the reasons for the fast water exchange rates measured in $[Gd(H_2O)(\mathbf{L^1})]$ and $[Gd(H_2O)(\mathbf{L^2})]^-$ complexes. The water exchange is fast despite the "unfavorable" SA structure, which predominates in solution.

Acknowledgment. We would like to thank Prof. É. Tóth and B. Drahoš (Orleáns, France) for a part of UV-vis measurements. Support from the Grant Agency of the Czech Republic (Grant 203/06/0467), the Grant Agency of the Academy of Science of the Czech Republic (Grant KAN201-110651), and the Long-Term Research Plan of the Ministry of Education of the Czech Republic (Grant MSM0021620857) is acknowledged. The work was carried out in the frame of COST D38 and the EU-supported NoE projects EMIL (Grant LSHC-2004-503569) and DiMI (Grant LSHB-2005-512146).

Supporting Information Available: Crystallographic file in CIF format; molecular peaks found in MS spectra of the complexes; HPLC characterization of prepared complexes; dihedral angles found in X-ray structures; molecular structure of $[Yb(\mathbf{L^1})]$ found in the crystal structure of $[Yb(\mathbf{L^1})]\cdot 4H_2O$; crystal packing found in the structure of $[Nd(H_2O)(\mathbf{L^1})]\cdot KCl\cdot HCl\cdot 7.5H_2O$; detailed view of two conformations of the six-membered chelate ring; definition of the axial protons in complexes of DOTA-like ligands; ^{1}H NMR spectra of Nd^{III}, Eu^{III}, and Yb^{III} complexes of $H_3\mathbf{L^1}$ and $H_4\mathbf{L^2}$ at variable temperatures; ^{1}H NMR EXSY spectrum of $[Eu(H_2O)(\mathbf{L^1})]$; absorption spectra of $[Eu(H_2O)(\mathbf{L^1})]$ at variable temperatures; plot of the relative intensities of the $^7F_0 \rightarrow {}^5D_0$ spectral bands of $[Eu(H_2O)(\mathbf{L^1})]$ vs temperature; plot of the half-widths and chemical shifts of the H231 ^{1}H NMR signal of $[Eu(H_2O)(\mathbf{L^1})]$ vs temperature; and representative HPLC chromatograms of prepared complexes. This material is available free of charge via the Internet at http://pubs.acs.org.

IC801597Z

(33) Lubal, P.; Vaněk, J.; Ševčíková, R.; Ševčík, R.; Huserová, J.; Polášek, M.; Hermann, P.; Kotek, J.; Lukeš, I. Unpublished results.